Mon. Not. R. astr. Soc. (1992) **255,** 129–145

Model atmospheres for neutron stars

M. C. Miller[1]★

[1] *Theoretical Astrophysics, California Institute of Technology, Pasadena, California 91125, USA*

Accepted 1991 October 2. Received 1991 August 28; in original form 1990 September 14

SUMMARY

While the presence of an atmosphere on a neutron star will not significantly modify its total thermal emission, it may change the emission in the sensitivity bands of detectors such as *Einstein* or *ROSAT* so that the inferred surface temperature (from a blackbody curve) may be quite different from the actual surface temperature. This in turn may affect deduced cooling curves. Previous calculations of model atmospheres of neutron stars have used atomic data calculated for zero magnetic field. However, many neutron stars are expected to have extremely high magnetic fields, on the order of $B \geq 10^{12}$ G, and it is important to take this into account. This paper uses atomic data in high magnetic fields computed using a multiconfigurational Hartree–Fock code, and the data were presented in Miller & Neuhauser. The effects of ionization and polarization in strong magnetic fields are discussed, and the prospects for observation by satellites are investigated.

1 INTRODUCTION

SN1987A is now nearly five years old, and as the expanding gas shell that surrounds it becomes optically thin, there is the possibility that a central neutron star will be observed. Because of its youth, this object would have a relatively high surface temperature, so that its thermal flux might be observable. Satellites such as *ROSAT* and *AXAF* may be able to detect such an object, and they have great enough sensitivity that they may be able to detect thermal radiation from other sources, such as the Crab or Vela pulsars. The determination of surface temperatures from X-ray observations will set constraints on the cooling curves of neutron stars, and thus will give valuable clues to the interior structure of these objects (see e.g. Tsuruta 1986). Preliminary models of neutron-star atmospheres (Romani 1987) indicate that even more stringent limits may be placed on the cooling curves, because the surface temperature inferred from the flux in the *Einstein* sensitivity band is much greater than the actual surface temperature. However, these models have not included the effect of magnetic fields.

There is overwhelming evidence, both direct and indirect, that many observable neutron stars have surface magnetic fields in excess of 10^{12} G. The indirect evidence includes models of radio pulsar slowdown as due to magnetic interactions [see Bhattacharya & van den Heuvel (1991) for a recent review] and models of the relation between luminosity and spin-rate behaviour for accretion-powered pulsars (Joss & Rappaport 1984; Nagase 1989). More direct evidence comes from the observation of cyclotron features in some X-ray sources (Kirk & Trümper 1983) and the recent discovery of paired cyclotron lines in some gamma-ray bursts (Murakami *et al.* 1988). Fields of this strength dominate the physics of the surface, and in particular they shift the energy levels of the atoms. A great deal of work has been done to compute the wavefunctions, energy levels and radiative cross-sections for hydrogen in high fields (e.g. Simola & Virtamo 1978; O'Connel 1979; Kara & McDowell 1980; Wunner, Ruder & Herold 1980; Rösner *et al.* 1983, 1984; Forster *et al.* 1984; Ruder *et al.* 1985; Wunner 1986; Wunner & Ruder 1987), and similar calculations have been done for helium and carbon (Miller & Neuhauser 1991, hereafter Paper I). The need to consider many different compositions is due to the large variety of processes that can contribute to the makeup of the surface. For example, iron could be the dominant element because current models predict that the mass cut of the supernova occurs in the iron layer. Hydrogen could be important because it is the most abundant element accreted once the neutron star starts interacting with the interstellar medium. Other elements such as helium or carbon could contribute, either because the neutron star might accrete from the supernova shells or because fusion may take place on the star's surface. For the purposes of this paper, what is important is the composition of the X-ray photosphere, and the situation is somewhat simplified because the lightest element present will dominate the soft X-ray opacity. An optical depth of unity in X-rays requires only about 10^{14} g of material (Romani 1987), and the surface gravity is high enough that gravitational separation will take place in only ~1–100 s (Alcock &

★ Present address: High Energy Physics, University of Illinois at Urbana-Champaign, Urbana, Illinois 61801, USA.

Illarionov 1980), so only pure-element photosphere compositions need be considered.

In this paper, we use cross-sections computed from the wavefunctions of atoms and ions in high fields ($\gtrsim 10^{12}$ G) to construct model atmospheres for neutron stars. The discovery of many old neutron stars with probable surface fields $B \approx 10^8$–10^{10} G makes modelling such stars an attractive problem. However, the code which generated the atomic data used in this paper assumes that the magnetic field dominates Coulomb interactions, so the code is not accurate at these intermediate field-strengths. We consider relatively low temperatures, $T = 3 \times 10^5$ to 10^6 K, consistent with the upper limits derived from X-ray observations. In Section 2, we describe our method for producing local thermodynamic equilibrium (LTE) models, including the Khersonskji (1987) high-field modification of the Saha ionization equation. Since the only source of opacity considered is bound–free, we make an estimate of the effects of bound–bound opacity and line broadening. We find that for $T \lesssim 3 \times 10^5$ K line broadening has a significant effect, so we concentrate on the upper end of the temperature range, $T = 10^6$ K. In Section 3, we produce spectra for several combinations of parameters and discuss the effect on observable lines of the variation of the magnetic field over the surface of the star, and in Section 4 we consider the effect of these results on colour temperatures and cooling curves.

2 MODEL ATMOSPHERES

2.1 Iteration procedure and temperature correction

The calculation of our LTE model atmospheres follows the standard treatment given by Mihalas (1978) for plane-parallel atmospheres. The assumption that the atmosphere is plane parallel is much better for neutron stars than for main-sequence stars, because for soft X-rays at optical depth unity, the atmosphere has a thickness < 1 cm, small compared to the neutron star radius of $\sim 10^6$ cm. The computation works on a grid of 100 zones, arranged logarithmically in Rosseland optical depth from 10^{-3} to 10^2. The iteration towards the temperature profile starts with an initial guess, taken as that of grey opacity,

$$T = T_0(\tau_R + q)^{1/4}, \tag{1}$$

where τ_R is the Rosseland optical depth and $q \approx 0.71044$ to ensure agreement with the exact grey solution at large depth. The photon frequencies are also arranged logarithmically, with 100 levels from 1 eV to 10 keV. Hydrostatic equilibrium is imposed by

$$\frac{dP}{d\tau_R} = \frac{g_s}{\kappa_R(\tau_R)}, \tag{2}$$

where g_s is the surface gravity, P is the pressure and κ_R is the Rosseland opacity. The equation of state is used to determine the density from the pressure. It is demonstrated in Section 2.3 below that, consistent with recent results from Abrahams & Shapiro (1991) an ideal-gas equation of state

$$P = nkT \tag{3}$$

should be accurate in the photosphere. Following Mihalas (1978), the flux is computed at each level of the atmosphere from

$$F_\nu(\tau) = 2\int_\tau^\infty B_\nu[T(t)]E_2(t-\tau)\,dt - 2\int_0^\tau B_\nu[T(t)]E_2(\tau-t)\,dt, \tag{4}$$

where $B[T(t)]$ is the Planck function and $E_2(t-\tau)$ is the second exponential function. Note that this assumes that the source function is equal to the Planck function. This is reasonably accurate, because in the frequency range considered, absorption dominates scattering.

The number density of neutral atoms, singly ionized atoms, etc. in each level of the atmosphere is determined by solving the ionization equation, and when the flux is calculated, the Lucy–Unsöld procedure is used to impose flux constancy. This method estimates the temperature correction at a given level by

$$\Delta T(\tau) \approx \frac{T(\tau)^{-3}}{16\sigma_R}\left\{\frac{\kappa_J}{\kappa_P}\left[3\int_0^\tau \frac{\kappa_F(\tau')}{\kappa_R(\tau')}\Delta F(\tau')\,d\tau + 2\Delta F(0)\right] - \frac{\kappa_R}{\kappa_P}\frac{d\Delta F(\tau)}{d\tau_R}\right\}, \tag{5}$$

where κ_R, κ_F, κ_P and κ_J are the Rosseland, flux, Planck, and absorption mean opacities, respectively. The approximation $\kappa_J = \kappa_P$ was found to give sufficient accuracy. After the new temperature profile is found, hydrostatic equilibrium is re-established, the ionization equations are solved again, a new flux table is computed, and the process is iterated. Five iterations are usually sufficient to produce flux constancy to within < 1 per cent throughout the atmosphere.

2.2 Line broadening in strong magnetic fields

In the high-density, high-temperature environment of a neutron star's atmosphere, spectral lines will be broadened substantially. Because of the complexities involved in an accurate calculation of broadening, this effect will be ignored in this paper. However, in this section some rough estimates are made to determine when line opacity is important.

Because the Rosseland mean opacity is weighted by the derivative of the Planck function with respect to temperature, dB_ν/dT, the greatest weight is put on frequencies near $\hbar\omega = 4kT$. We consider as an example transitions involving the outer, hydrogen-like electron of a neutral atom. It was demonstrated in Paper I that the energy levels of these outer electrons are close to independent of the atomic number, so this treatment should be representative of the effects of line broadening on the opacity below ≈ 300 eV. The specific transition considered is from the ground state to the first excited state, so the line centre is at about 150 to 250 eV if the magnetic field is between $B = 10^{12}$ and 5×10^{12} G. If the temperature is between $T = 10^5$ and 10^6 K, the greatest weight is put on $\hbar\omega = 4kT \approx 30$ to 350 eV, which is, on average, ~ 10–100 eV away from the centre of the line. Whilst it is possible that, at a particular spot on the star's surface, the thermal peaks and line-centre wavelengths may be coincident, the expected variation of magnetic-field strength over the surface of the star and the dependence of electron binding energies on the magnetic field indicate that, over most of the surface, the centre of the line will be well away from the thermal peak. For example, if a neutron star

has a purely dipolar field with an equatorial strength of 2.35×10^{12} G, then the ground-state binding energy of hydrogen would vary from 208 eV at the equator to 253 eV at the poles (see Paper I). Thus, collisional broadening (which is most important in line wings) is likely to dominate over Doppler broadening (which has its largest effect on line cores). The opacity at this frequency from bound–bound transitions will be compared to the opacity from bound–free transitions, so that an order-of-magnitude estimate of the importance of bound–bound transitions may be made.

The assumption is made that the change in frequency that is due to an encounter may be described by the Weisskopf approximation

$$\Delta\omega=\frac{C_p}{r^p}, \tag{6}$$

where r is the distance between the atom and perturber, and for example $p=2$ is appropriate for the linear Stark effect, whereas $p=3$ represents resonance broadening. It is assumed that when the frequency is within some critical frequency of the line centre,

$$\Delta\omega<\Delta\omega_g, \tag{7}$$

the cross-section has a Lorentz form,

$$\sigma\propto\frac{1/2\pi\tau}{(\Delta\omega)^2+(1/2\tau)^2}, \tag{8}$$

where τ is the mean time between collisions. The critical frequency $\Delta\omega_g$ is assumed to be the Weisskopf frequency

$$\Delta\omega_g\approx\Delta\omega_w=\left(\frac{v^p}{C_p\psi_p^p}\right)^{1/p}, \tag{9}$$

where ψ_p is a phase shift: $\psi_2=\pi$, $\psi_3=2$. Outside this frequency, $\Delta\omega>\Delta\omega_g$, it is assumed that statistical broadening theory is applicable. The frequency dependence is different in a neutron star atmosphere than in laboratories, because the strong magnetic field constrains the atoms, ions and electrons to move in one dimension. It is therefore necessary to rederive $\sigma(\Delta\omega)$ in one dimension, and this is now done using the approximation that the nearest neighbour is responsible for the frequency shift.

To correspond with the standard derivation for three dimensions, a uniform particle density will be assumed. In reality, there are probably repulsive terms present. However, these are likely to be significant only when the size of the atoms is comparable to the mean separation between atoms. As is argued in Section 2.3, this density is unlikely to be reached in the photosphere, so the assumption of uniform particle density is adequate for the present purposes. Using this assumption, the probability $W(r)$ that the nearest neighbour lies at a distance r is

$$W(r)=n_1e^{-rn_1}. \tag{10}$$

Here n_1 is the linear number density of the perturbers along the field line, so that if the number density is n cm^{-3} and the area of the magnetic flux tube is A cm^2, then $n_1=nA$ cm^{-1}. Here A is roughly given by

$$A=\pi\hat{\rho}^2,$$

where

$$\hat{\rho}=\left(\frac{\hbar c}{eB}\right)=2.5\times10^{-10}\frac{B}{10^{12}\text{ G}}\text{ cm} \tag{11}$$

is the radius of the first Landau level. Defining the normal phase shift $\Delta\omega_0$ by

$$\Delta\omega_0=\frac{C_p}{r_0^p}, \tag{12}$$

where r_0 is the mean interparticle distance $r_0=1/n_1$, we see that

$$\left(\frac{\Delta\omega}{\Delta\omega_0}\right)^{1/p}=\frac{r_0}{r}. \tag{13}$$

Setting $\beta=\Delta\omega/\Delta\omega_0$ and substituting, equation (10) becomes a statement about the distribution of frequencies from an initially sharp line:

$$W(\beta)\,d\beta=\frac{1}{p}\beta^{(-1-1/p)}\exp(-\beta^{-1/p})\,d\beta. \tag{14}$$

This compares with the three-dimensional value of

$$W(\beta)\,d\beta=\frac{3}{p}\beta^{(-1-3/p)}\exp(-\beta^{-3/p})\,d\beta, \tag{15}$$

so in the presence of a strong magnetic field, the line opacity drops off less sharply. The cross-section integrated over all frequencies is

$$\int_0^\infty\sigma\,d\omega=\frac{2\pi^2e^2}{mc}f, \tag{16}$$

where the oscillator strength $f\approx1$. Using this and the assumptions above, the line cross-section for $\Delta E>1$ eV and $n_7<1$, where ΔE is the 'distance' from the line centre and $n_1=10^7n_7$ cm^{-1} is:

Stark broadening;

$$\sigma_S\approx3\times10^{-18}n_7c_2^{1/2}\left(\frac{\Delta E}{1\text{ eV}}\right)^{-3/2}\text{ cm}^2, \tag{17}$$

Resonance broadening;

$$\sigma_R\approx8\times10^{-19}n_7c_3^{1/3}\left(\frac{\Delta E}{1\text{ eV}}\right)^{-4/3}\text{ cm}^2. \tag{18}$$

In these expressions, c_2 and c_3 are, respectively, the ratio of the one-dimentional Stark constant to the three-dimensional Stark constant, and the ratio of the one-dimensional resonance constant to the three-dimensional resonance constant. In three dimensions, the Stark constant is $C_2\approx1$ cm^2 s^{-1} and the resonance constant is $C_3\approx5\times10^{-10}$ cm^3 s^{-1}. The true values of c_2 and c_3 can only be determined by experiment or a detailed quantum-mechanical calculation, so it is impossible to determine *a priori* the magnitudes of c_2 and c_3. However, the low powers of c_2 and c_3 in expressions (17) and (18) diminish the impact of their potential differences from unity.

To compare the bound–bound cross-section to the bound–free cross-section, we take as an example hydrogen at

$B = 10^{12}$ G. Here σ_s and σ_R are respectively the Stark and resonance cross-sections of the transition $(m=0,\ \nu=0)$ to $(m=0,\ \nu=1)$ at the frequency $\hbar\omega = 4kT$. This is compared to the combined ionization cross-sections σ_{bf} from the $(m=0,\ \nu=0)$ and $(m=0,\ \nu=1)$ states. The densities that are used to calculate σ_S and σ_R are the densities at unit Rosseland optical depth, which were calculated without including the line opacities. At $B = 10^{12}$ G, the excitation energy of the $(m=0,\ \nu=1)$ state is 145 eV, so this state is assumed to have $e^{-145\ \mathrm{eV}/kT}$ of the population of the ground state, and $\Delta E = |145\ \mathrm{eV} - 4kT|$. The bound–free cross-sections were computed using code described in Paper I, which used a formalism partially expressed by equations (47) and (49).

At $T = 10^5$ K $\Rightarrow 4kT = 34.6$ eV;

$\rho = 120\ \mathrm{g\ cm^{-3}} \Rightarrow n_7 = 2.4$, $\sigma_S \approx 6\times10^{-21} c_2^{1/2}\ \mathrm{cm^2}$,

$\sigma_R \approx 4\times10^{-21} c_3^{1/3}\ \mathrm{cm^2}$, $\sigma_{bf} \approx 4\times10^{-21}\ \mathrm{cm^2}$.

At $T = 3\times10^5$ K $\Rightarrow 4kT = 104$ eV;

$\rho = 0.4\ \mathrm{g\ cm^{-3}} \Rightarrow n_7 = 0.008$, $\sigma_S \approx 9\times10^{-23} c_2^{1/2}\ \mathrm{cm^2}$,

$\sigma_R \approx 4\times10^{-23} c_3^{1/3}\ \mathrm{cm^2}$, $\sigma_{bf} \approx 1\times10^{-22}\ \mathrm{cm^2}$.

At $T = 10^6$ K $\Rightarrow 4kT = 346$ eV;

$\rho = 0.2\ \mathrm{g\ cm^{-3}} \Rightarrow n_7 = 0.004$, $\sigma_S \approx 4\times10^{-24} c_2^{1/2}\ \mathrm{cm^2}$,

$\sigma_R \approx 3\times10^{-24} c_3^{1/3}\ \mathrm{cm^2}$, $\sigma_{bf} \approx 4\times10^{-20}\ \mathrm{cm^2}$.

From this, it is apparent that if c_2 and c_3 are close to unity then lines may have a very significant effect at low temperatures (because of the lack of other opacity sources), but that at high temperatures they may be ignored. The high-temperature result is almost rigorous, because the ratio of cross-sections is so high; c_2 would have to be at least 10^8, and c_3 would have to be at least 10^{12}, for line broadening to be important. Because of the likely loss of accuracy at low temperatures, the models in Sections 3 and 4 concentrate on $T > 3\times10^5$ K.

2.3 Equation of state in the atmosphere

In this paper the equation of state in the photosphere is assumed to be that of an ideal gas. Recent work by Abrahams & Shapiro (1991) has supported this approximation, and in this section this assumption is justified by showing that in the photosphere the contributions to the pressure from electron degeneracy and ion corrections are negligible.

For a degenerate electron gas in one dimension, the number of states in a volume V and a range of z momenta Δp_z is given by

$$n = \frac{eBV\Delta p_z}{h^2 c} \tag{19}$$

(Landau & Lifshitz 1977), so the density and pressure are given by

$$n_e = \frac{eB}{h^2 c}\int_{-\infty}^{\infty} f\,dp_z \tag{20}$$

and

$$P = \frac{eB}{h^2 c}\int_{-\infty}^{\infty} pvf\,dp_z, \tag{21}$$

and for complete degeneracy the occupation number f is

$$f = 1 \text{ for } |p| \le p_F, \qquad f = 0 \text{ for } |p| > p_F, \tag{22}$$

where p_F is the Fermi momentum. Therefore,

$$n_e = \frac{2eB}{h^2 c} p_F. \tag{23}$$

The energies considered are much less than the electron rest mass m, so $v \approx p/m$ and

$$P \approx \frac{2eB}{3h^2 cm} p_F^3 \approx 7\times10^{17} B_{12}^{-2} n_{27}^3\ \mathrm{N\ cm^{-2}}, \tag{24}$$

where $B = 10^{12} B_{12}$ G and $n_e = 10^{27} n_{27}\ \mathrm{cm^{-3}}$. The pressure of an ideal gas is

$$P = nkT \approx 10^{17} n_{27} T_6\ \mathrm{N\ cm^{-2}}, \tag{25}$$

where the temperature is $T = 10^6 T_6$ K, so the two are equal at about $n_{27} = 0.4$ and degeneracy pressure may be ignored when $n_{27}^2 \ll 1$.

The interactions between atoms become important when the mean distance between atoms is comparable to the size of the ions. The outer electron of a neutral atom of atomic number Z in a strong magnetic field has an orbital radius of

$$\rho = \sqrt{(2Z-1)}\,\hat{\rho}$$

and a length along the field of (Miller & Neuhauser 1991)

$$l \approx \left[\frac{a_0/\hat{\rho}}{\ln(a_0/\hat{\rho})}\right]\hat{\rho}, \tag{26}$$

where a_0 is the Bohr radius, $a_0 = 5\times10^{-9}$ cm. The average distance between atoms is

$$r \approx \frac{1}{nA}, \tag{27}$$

where $A = \pi\rho^2 = \pi(2Z-1)\hat{\rho}^2$. The condition $r \gg l$ then yields $n_{27} \ll 5/(2Z-1)$.

In order to determine whether these conditions are satisfied, it is necessary to estimate the number density in the photosphere. This may be done from the equation of hydrostatic equilibrium (2), which can be written in the form

$$\frac{dP}{d\tau} = \frac{g_s}{\sigma/\mu}, \tag{28}$$

where σ is some average cross-section and μ is the mass of an atom. This may be directly integrated, and if an ideal-gas equation of state $P = nkT$ is assumed, the number density is

$$n = \frac{g_s}{kT\sigma/\mu}\tau. \tag{29}$$

For typical values $g_s = 3\times10^{14}\ \mathrm{cm\ s^{-2}}$, $T = 10^5$ K, $\sigma = 10^{-21}\ \mathrm{cm^2}$ and $\mu = 10^{-23}$ g, the number density at the lower extreme of the atmosphere, $\tau = 100$, is $n = 2\times10^{25}\ \mathrm{cm^{-3}}$. Therefore, the conditions above are satisfied, and to a good approximation the equation of state is that of an ideal gas. Fig. 1 compares the pressures given by various equations of

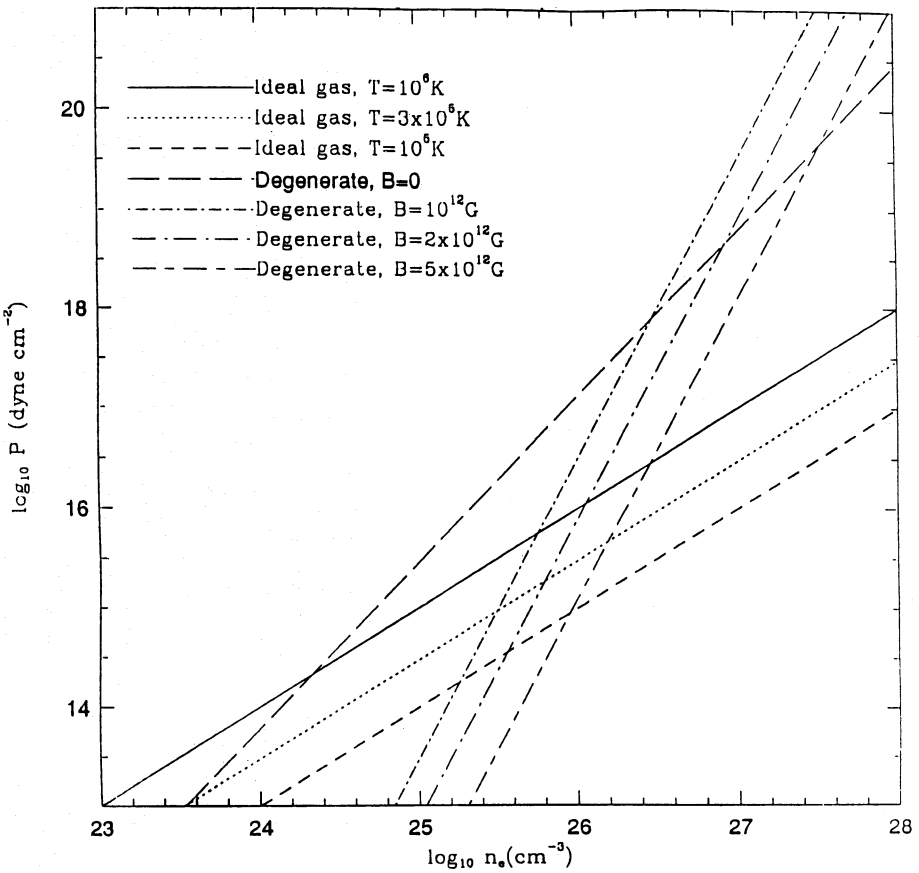

Figure 1. A comparison of the pressures given by: an ideal gas; electron degeneracy at a magnetic field $B=0$; and electron degeneracy at a magnetic field $B=10^{12}$ G, as a function of electron density n_e.

state at a variety of values of the electron density. From this diagram, it is evident that the strong magnetic field plays an important part in the non-degeneracy of the atmosphere, and if the magnetic field were to decay away, the pressure would be dominated by electron degeneracy. Furthermore, at a frequency which has very low cross-section (such as the higher frequencies in our model, $\omega \sim 10$ keV), the density at optical depth unity may be high enough that degenerate pressure is important at the 10 per cent level.

2.4 High-field ionization

For a general multi-electron atom, it is necessary to determine the number densities of all of the various ions of the atom. Khersonskij (1987) derived a high-field ionization equation to replace the Saha equation for hydrogen.

For a hydrogen atom, the neutral hydrogen density n_H at temperature T and magnetic field B is determined by

$$\frac{n_H}{n_p n_e} = \frac{1}{2}\left(\frac{2\pi\hbar^2}{m_e kT}\right)^{3/2} \frac{\sinh \eta_p}{\eta_p} \frac{\coth \eta_e}{\eta_e} e^{E_a/kT} f_H(B, T), \qquad (30)$$

where n_p is the proton density, n_e is the electron density, m_e is the mass of the electron, $\eta_p = \hbar\omega_p/2kT$, where ω_p is the cyclotron frequency, $\omega_p = eB/m_p c$, $\eta_e = \hbar\omega_e/2kT$, E_a is the magnitude of the ground-state energy, and the partition function f_H is given by

$$f_H(B, T) = \sum_{s=0}^{\infty} \exp\left(-\frac{E_a + \varepsilon_s + m\hbar\omega_p}{kT}\right), \qquad (31)$$

where ε_s is the energy of the sth excited state, $\varepsilon_s < 0$, and $m\hbar\omega_p$ is the correction for finite proton mass, where m is the azimuthal quantum number.

For $Z > 1$, the natural generalization (corresponding to the Saha equation) is to replace m_p with m_N, the mass of the nucleus, and replace

$$\frac{n_H}{n_p n_e} \qquad (32)$$

with

$$\frac{n_r}{n_{r+1} n_e}, \qquad (33)$$

where n_r is the number density of the r-times-ionized ion.

For hydrogen, one can calculate the ionized fraction,

$$x_p = \frac{n_p}{n_t} = 1 - x_H, \qquad (34)$$

where n_t is the total density of baryons, from

$$x_p = \sqrt{\left[\frac{1}{4(Kn_t)^2} + \frac{1}{Kn_t}\right]} - \frac{1}{2Kn_t}, \quad (35)$$

where

$$K \equiv \frac{n_H}{n_p n_e}.$$

For example, for $B = 10^{12}$ G and $T = 10^5$ K, $x_p = 0.058$, whereas for $B = 10^{13}$ G and $T = 10^6$ K, $x_p = 2.2 \times 10^{-5}$, all assuming a total number density of $n_t = 10^{21}$ cm^{-3}.

For an atom with atomic number Z, the ionization equations are of the form

$$\frac{n_r}{n_{r+1} n_e} = K_r, \quad (36)$$

where K_r is a constant given by the equations above. The total number density is

$$n_t = n_0 + n_1 + \ldots + n_Z, \quad (37)$$

and charge conservation gives

$$n_e = n_1 + 2n_2 + \ldots + Zn_Z. \quad (38)$$

These equations are solved by an iterative averaging method, which provides convergence at a level of 10^{-5} in less than 10 steps.

Numerically, it is found that for hydrogen at $\rho = 1$ g cm^{-3} (appropriate for $\tau_R = 1$) and $T < 6 \times 10^5$ K, an increase in magnetic field causes a decrease in ionization, while for $T > 6 \times 10^5$ K, an increase in B causes an increase in ionization. This is because as the field increases, the binding energy increases but the phase space decreases, and at $T \approx 6 \times 10^5$ K the two effects balance. However, for atoms with $Z > 1$ at $T < 10^6$ K, an increase in magnetic field causes a decrease in ionization. Figs 2(a–d) show the fractions of neutral atoms at various values of the magnetic field and temperature for hydrogen, helium, carbon and nitrogen.

Therefore, for a given magnetic field, temperature, and total number density, the number densities of the ions may be calculated. For a given ion, it is assumed that the ground state and excited states are distributed according to a Boltzmann law,

$$n \propto e^{-E/kT}. \quad (39)$$

3 SPECTRA

Model atmospheres have been calculated for surface compositions of pure hydrogen, pure helium, pure carbon and pure nitrogen at equatorial magnetic fields of 9.4×10^{11} 2.35×10^{12} and 4.7×10^{12} G (these values for B are multiples of the critical field at which magnetic effects dominate for the ground state of hydrogen, 2.35×10^9 G). Because the magnetic field varies over the surface of the star, it is important to account for this effect. It is also interesting to investigate the importance of polarization; these effects are considered in the following sections.

3.1 Interpolation of model atmospheres

If we assume that neutron stars have roughly dipolar magnetic fields, then the strength of the field varies by a factor of 2 from the magnetic equator to the magnetic pole. The presence of higher multipoles would create an even larger variation in the magnetic field. Since for our calculations we assume that the field is of such a strength that it dominates the energetics of the atom, the energy levels of atoms will be shifted dramatically between the equator and the poles. In order to account for this, it would seem reasonable to calculate cross-section-versus-frequency tables for many intermediate field-strengths, then sum these over the surface of the star, appropriately weighted by projected area. However, the calculation of cross-section tables for a given magnetic field B and atomic number Z is a process that takes several hours, and would be computationally more intensive than desirable. It is therefore worthwhile to search for approximations at intermediate fields.

The approximation we will make is that the cross-sections are shifted in frequency by the amount that the ground-state energy level changes, and in magnitude such that the integrated cross-section is constant;

$$\int \sigma(B_1, \nu)\, d\nu = \int \sigma(B_2, \nu)\, d\nu. \quad (40)$$

Another way of saying this is that we assume that the oscillator strength of a given transition, $f = (mc/\pi e^2) \int \sigma\, d\nu$, is roughly constant with respect to magnetic field. For example, the ground-state binding energy for hydrogen at 2.35×10^{12} G is 208 eV, while at 4.7×10^{12} G it is 253 eV. Thus, we would assume that for hydrogen

$$\sigma\left(B = 4.7 \times 10^{12}\ \text{G}, \frac{253}{208}\nu\right) = \frac{208}{253}\sigma(B = 2.35 \times 10^{12}\ \text{G}, \nu), \quad (41)$$

where $\sigma(B, \nu)$ is the cross-section as a function of magnetic field and frequency. In order to make this approximation relevant to ions with $Z > 1$, we work from the Ruderman scaling formula $E \sim \ln^2(B/Z^2 B_c)$, where B_c is the critical field, $B_0 = 2.35 \times 10^9$ G in Ruderman's derivation, but in our case B_c is determined from numerical simulations. Between 2.35×10^{12} and 4.7×10^{12} G, the best fit to hydrogen ground-state energies is given by $B_c = 2.8 \times 10^9$ G. Therefore, the ratio of the binding energy at an intermediate field, B_{int}, to the binding energy at the low field, $B_{low} = 2.35 \times 10^{12}$ G, is given approximately by

$$\frac{E_{int}}{E_{low}} \approx \frac{\ln^2[B_{int}/(Z^2 B_0)]}{\ln^2[B_{low}/(Z^2 B_0)]}, \quad (42)$$

and our estimate for the cross-section at intermediate field is

$$\sigma\left(B_{int}, \frac{E_{int}}{E_{low}}\nu\right) = \sigma(B_{low}, \nu). \quad (43)$$

This approximation assumes that the scaling of energies is hydrogenic. This is fairly accurate for the outer electron of an atom, but breaks down for the inner electrons. However,

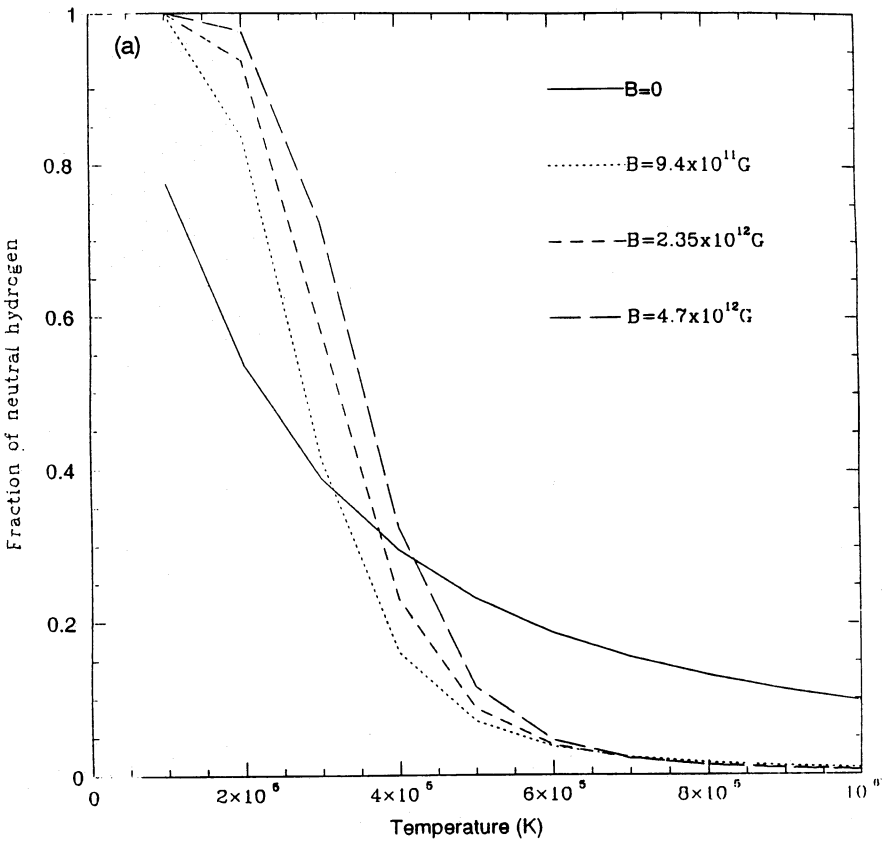

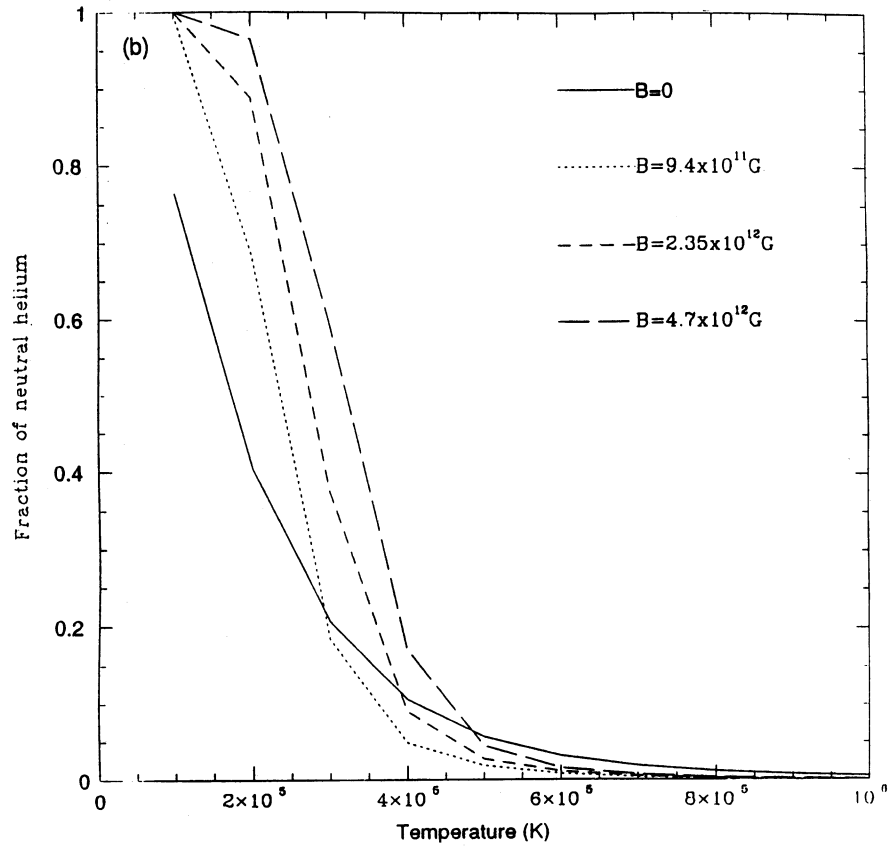

Figure 2. The fraction of neutral atoms at a density of $\rho = 1$ g cm^{-3} for (a) hydrogen, (b) helium, (c) carbon and (d) nitrogen at a variety of temperatures and magnetic fields. The ionization fraction at $B = 0$ is included for comparison.

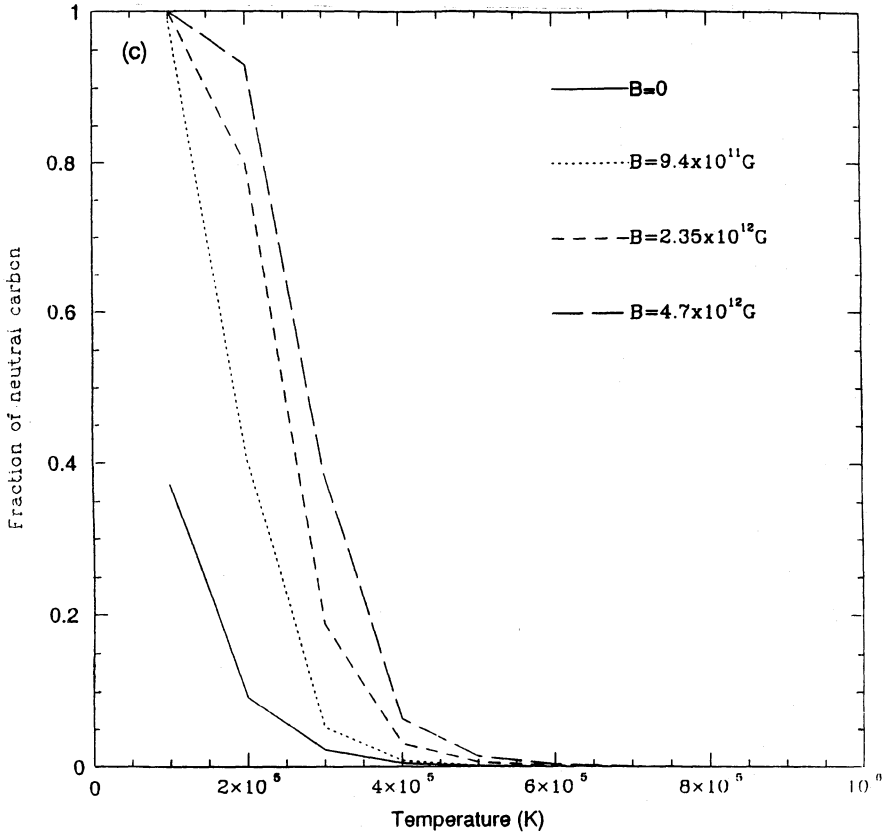

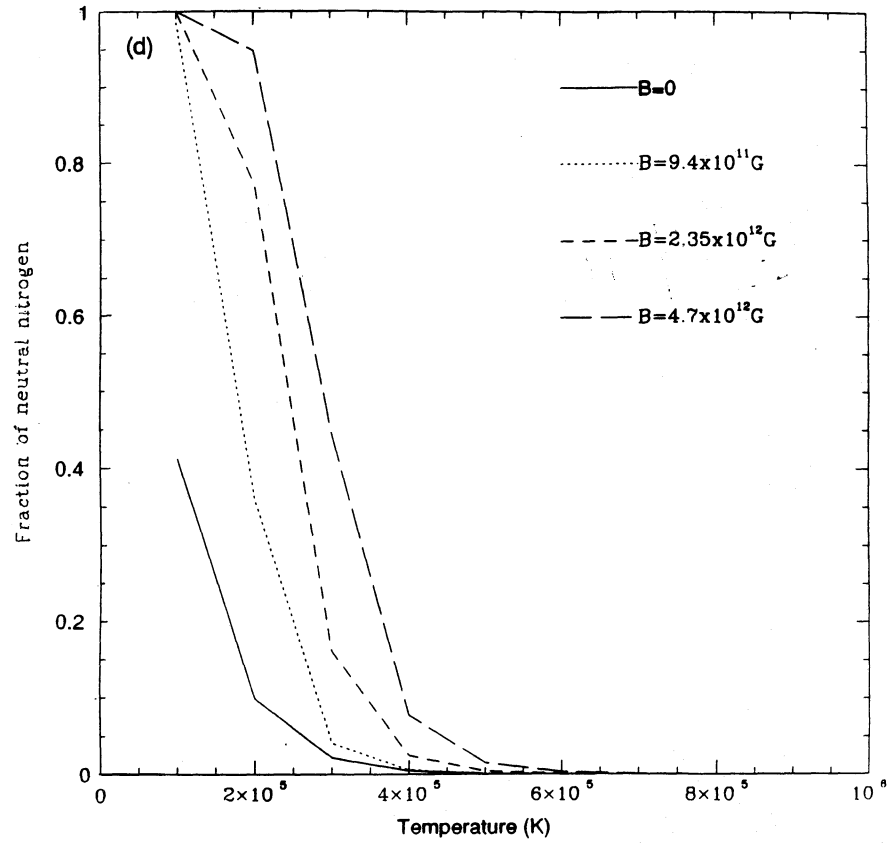

Figure 2 – *continued*

this should not detract significantly from the computations because the ionization energies of the inner electrons are in the several hundred eV range, which is substantially higher than the typical photon energy $\hbar\omega \sim 10$–100 eV from a thermal bath at $T \sim 10^5$–10^6 K.

3.2 Effects of polarization

Calculations of radiative cross-sections in strong magnetic fields, as might be found on the surface of a neutron star, have used the implicit assumption that if the radiation field is isotropic and unpolarized, then all polarization components will make equal contributions to the cross-section. However, as indicated below, for bound–free interactions the component of polarization that is linear and parallel to the magnetic-field axis (which we call the B polarization) is dominant. In this section, we first give an estimate of the ratio of the cross-sections due to B and circular polarizations (where 'circular' is defined with respect to the direction of the field, not to propagation direction of the photon), then estimate the impact of this ratio on the ionization process.

In a strong magnetic field, an atom is stretched along the field, with its length-scale across the field given by

$$\hat{\rho} \approx 2.5 \times 10^{-10} B_{12}^{-1/2} \text{ cm}, \tag{44}$$

where $B_{12} = B/10^{12}$ G and its length-scale along the field given by

$$l \approx \left[\frac{a_0/Z\hat{\rho}}{\log(a_0/Z\hat{\rho})}\right]\hat{\rho}, \tag{45}$$

where a_0 is the Bohr radius, $a_0 \approx 5 \times 10^{-9}$ cm, and Z is the atomic number of the atom. For example, for $Z=1$ and $B_{12}=1$, $l \approx 7\hat{\rho}$. Henceforth we will consider the hydrogen atom, $Z=1$. We will use a cylindrical coordinate system, where z is the coordinate for the cylindrical axis, ρ is the radial coordinate, Φ is the azimuthal coordinate, and ν, n and m are their respective quantum numbers. We assume that the magnetic field is strong enough that all of the electrons are in their lowest Landau level, $n=0$. This is a fine approximation for neutron stars with $B \gtrsim 10^{12}$ G (see Paper I for details), but for magnetic fields near the critical field $B = 2.35 \times 10^9\ Z^2$ G, mixing with $n>0$ states must be considered. The atomic data used in this paper were generated using a code which assumed $n=0$, so low-field neutron stars cannot be treated accurately by the program described in Paper I. Given the large number of pulsars with inferred surface fields $B \approx 10^8$–10^{10} G, it would be a worthwhile future project to account for the $n>0$ states in models of such objects.

It is intuitively reasonable that for bound–free absorption, the B polarization should have a greater cross-section than the circular polarization, because it is interacting with the long axis of the atom. To get an idea of how great the difference is, we will look at Coulomb wavefunctions in the limit of low kinetic energy, $E = p^2/2M$. In a strong field, the Schrödinger equation along the field is

$$-\frac{\hbar^2}{2m}\frac{\partial^2\psi}{\partial z^2} - \frac{e^2}{z}\psi = E\psi.$$

Using the substitutions

$$\rho = \frac{\sqrt{2mE}}{\hbar} z, \qquad -2\eta = \frac{e^2}{\hbar}\sqrt{\frac{2m}{E}},$$

this becomes

$$\frac{d^2g}{d\rho^2} + \left(1 - \frac{2\eta}{\rho}\right) g = 0,$$

where $g(z)$ is the z-component of the wavefunction. This is the differential equation for the Coulomb functions, and in the limit $\rho \to 0$ and $\eta \to -\infty$ this becomes (see e.g. Abramowitz & Stegun 1972)

$$g(z) \approx \frac{z}{a_0} - \left(\frac{z}{a_0}\right)^2, \tag{46}$$

where $g(z)$ is the unbound wavefunction of the electron (this approximation is valid for $z < a_0$).

The circular cross-section is given by

$$\begin{aligned}\sigma_+ &\propto \left|\hat{\rho}\int_{-\infty}^{\infty} f_{m\nu}(z) g(z)\, dz\right|^2 \\ &= \left|\hat{\rho}\int_{-\infty}^{\infty} \mathrm{e}^{-|z|/l}\left[\frac{z}{a_0} + \left(\frac{z}{a_0}\right)^2\right] dz\right|^2, \\ &= \left|\frac{\hat{\rho}}{a_0}\int_{-\infty}^{\infty} \mathrm{e}^{-|z|/l}\,\frac{z^2}{a_0}\, dz\right|^2,\end{aligned} \tag{47}$$

where $f_{m\nu}(z)$ is the z-component of the bound wavefunction of the electron. Only the ground state is considered,

$$f_{m\nu} = f_{00} \approx \mathrm{e}^{-|z|/l}. \tag{48}$$

Similarly, the B polarization cross-section is

$$\begin{aligned}\sigma_B &\propto \left|\int_{-\infty}^{\infty} z f_{m\nu}(z) g(z)\, dz\right|^2 \\ &= \left|\int_{-\infty}^{\infty} z\,\mathrm{e}^{-|z|/l}\left[\frac{z}{a_0} + \left(\frac{z}{a_0}\right)^2\right] dz\right|^2 \\ &= \left|\int_{-\infty}^{\infty} \mathrm{e}^{-|z|/l}\,\frac{z^2}{a_0}\, dz\right|^2.\end{aligned} \tag{49}$$

Therefore, the ratio is

$$\frac{\sigma_B}{\sigma_+} \approx \left(\frac{a_0}{\hat{\rho}}\right)^2, \tag{50}$$

which has a value of about 400 for $B = 10^{12}$ G. This compares to a numerically determined value of about 10 000 at the absorption edge, where the greater value is due to the increased binding energy in a strong magnetic field. The approximations used above are valid for

$$E \ll E_{\text{ground}}, \tag{51}$$

where E is the kinetic energy of the free electron and $E_{\rm ground}$ is the ground-state binding energy of the atom, about 160 eV for $B=10^{12}$ G. In practice, the cross-section that is due to B polarization remains much greater than that due to circular polarization even at higher energies, so that, for example, at $B=4.7\times10^{12}$ G, $E=1000$ eV, $\sigma_B=5.4\times10^{-21}$ cm^2 and $\sigma_+=2.4\times10^{-25}$ cm^2. A similar ratio holds for ionization from excited states, so that it is a good approximation to assume that $\sigma_B \gg \sigma_+$ for all frequencies considered.

The total bound–free cross-section has the form

$$\sigma_{\rm bf} \sim \gamma_+ \sigma_+ + \gamma_- \sigma_- + \gamma_B \sigma_B, \quad (52)$$

where γ_+, γ_- and γ_B are the fractions of the light polarized in the right-circular, left-circular and magnetic-field directions, respectively. A calculation done for a dipolar field indicates (see Appendix A) that in a strong field $\gamma_B \approx 0.4$, and since for $\sigma_B \gg \sigma_+$

$$\sigma_{\rm bf} \approx \gamma_B \sigma_B,$$

the total cross-section is about 20 per cent greater than if the γs were equal.

It was determined that the surface gravity has a small effect on the unredshifted spectrum, as was also true in the non-magnetic case (Romani 1987). In Fig. 3 we see that the emergent spectrum for helium is very similar for surface gravities of 10^{14} and 10^{15} cm, s^{-2} for $B=4.7\times10^{12}$ G and surface temperature of 3×10^5 K. As in the non-magnetic case, what change there is in the spectrum is probably due to increased pressure ionization below the absorption edges in the high-gravity case. In the other spectra presented below, a surface gravity of 3×10^{14} cm s^{-2} is assumed.

Figs 4–7 show the unredshifted spectra from atmospheres with varying compositions and magnetic fields at an effective temperature of $T=10^6$ K. Fig. 8 shows the temperature as a function of Rosseland optical depth for carbon at $T=10^6$ K with various magnetic fields, and the relationship between temperature and optical depth is very similar for other compositions. Fig. 9 shows the pressure as a function of Rosseland optical depth for carbon at $T=10^6$ K with varying magnetic fields, and other compositions give similar results.

4 COLOUR TEMPERATURES AND COOLING CURVES

Table 1 lists the blackbody temperatures associated with the various magnetic field values and surface compositions of the model atmospheres. In this table, $T_{\rm E}$ is defined as the temperature of the blackbody curve which gives the same number of counts as the model atmosphere in the sensitivity range of the *Einstein* IPC (0.5 to 5.0 keV), while $T_{\rm R}$ is defined similarly for the *ROSAT* HRI (0.1 to 2.0 keV). Here the response curve for the *Einstein* IPC is taken from Harnden *et al.* (1984) and the response curve for the *ROSAT* HRI is taken from the *ROSAT Mission Description* (1989), table 4.4. We note that the ratio of blackbody temperature to effective

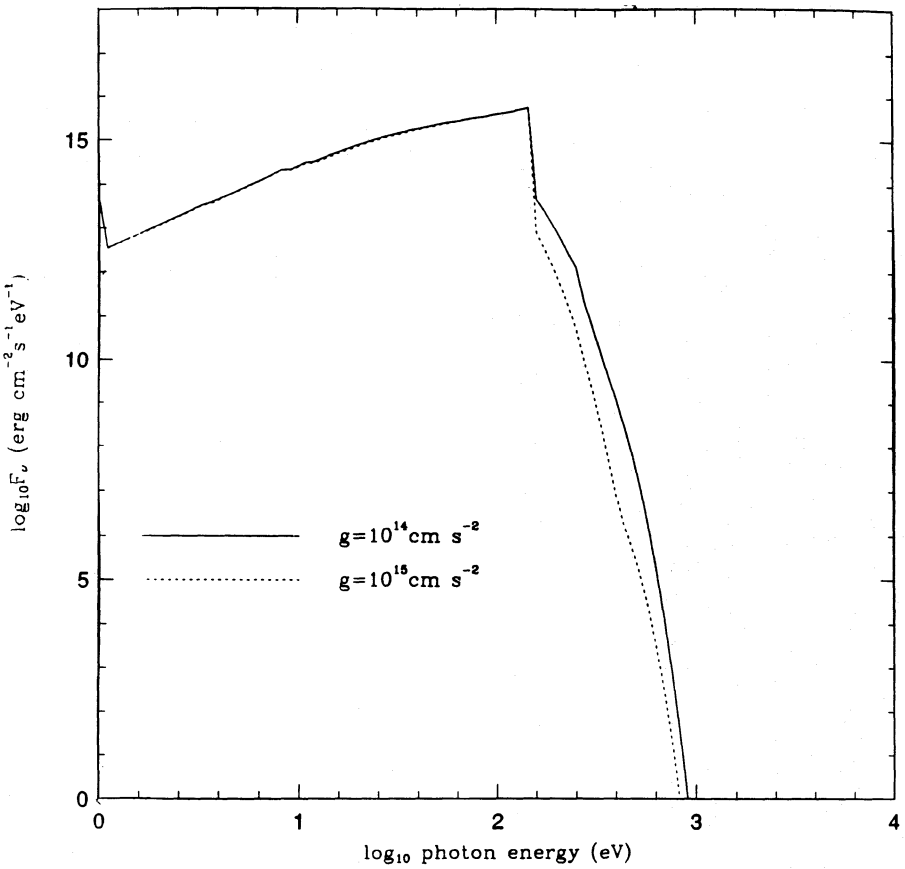

Figure 3. A comparison of the unredshifted spectra of helium at surface gravities of 10^{14} and 10^{15} cm s^{-2} for $B=4.7\times10^{12}$ G and $T=3.0\times10^5$ K. This figure demonstrates that the surface gravity does not have a significant effect on the unredshifted spectrum, and as a result we have set $g=3\times10^{14}$ cm s^{-2} in the calculations listed in Table 1.

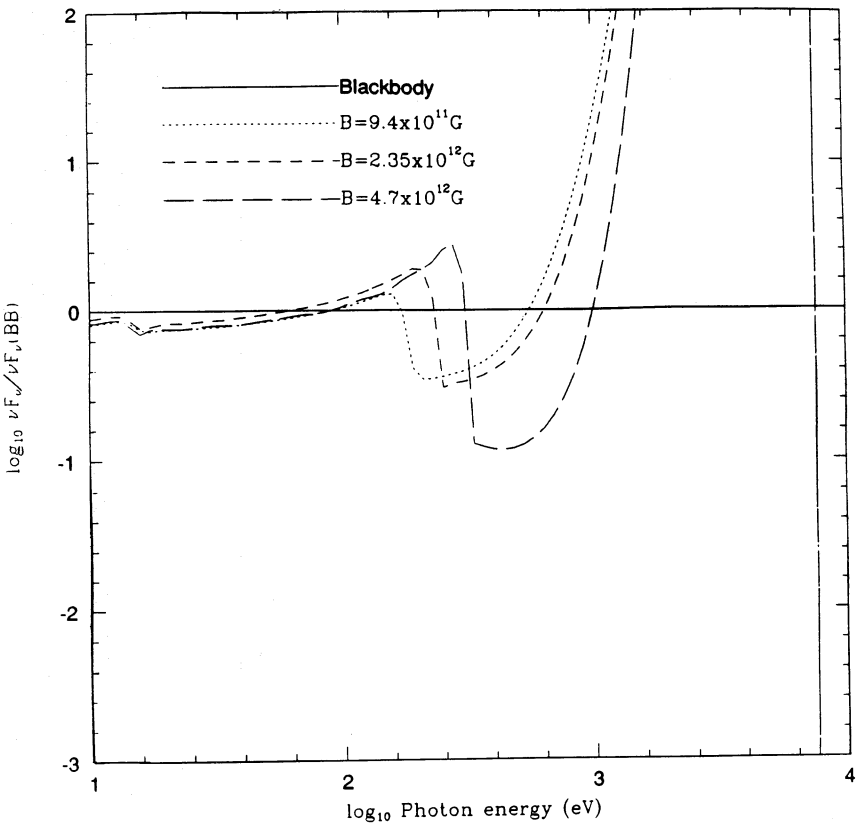

Figure 4. The ratio of the unredshifted spectrum of hydrogen to the spectrum of a blackbody at $T_{\rm eff} = 1.0 \times 10^6$ K and $B = 9.4 \times 10^{11}$, 2.35×10^{12} and 4.7×10^{12} G.

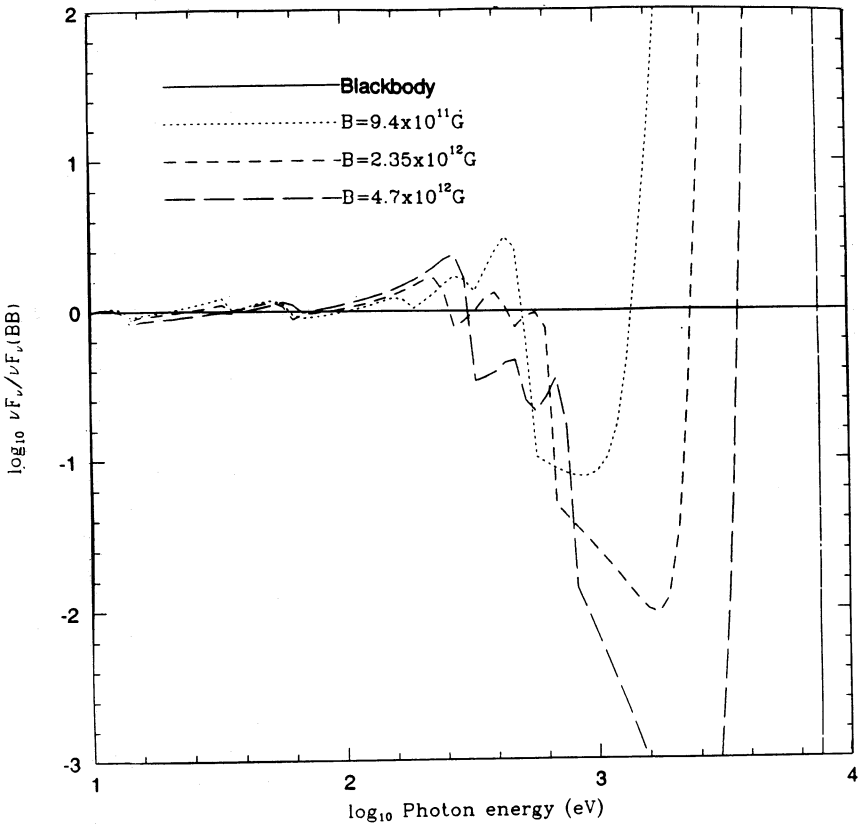

Figure 5. The ratio of the unredshifted spectrum of helium to the spectrum of a blackbody at $T_{\rm eff} = 1.0 \times 10^6$ K and $B = 9.4 \times 10^{11}$, 2.35×10^{12} and 4.7×10^{12} G.

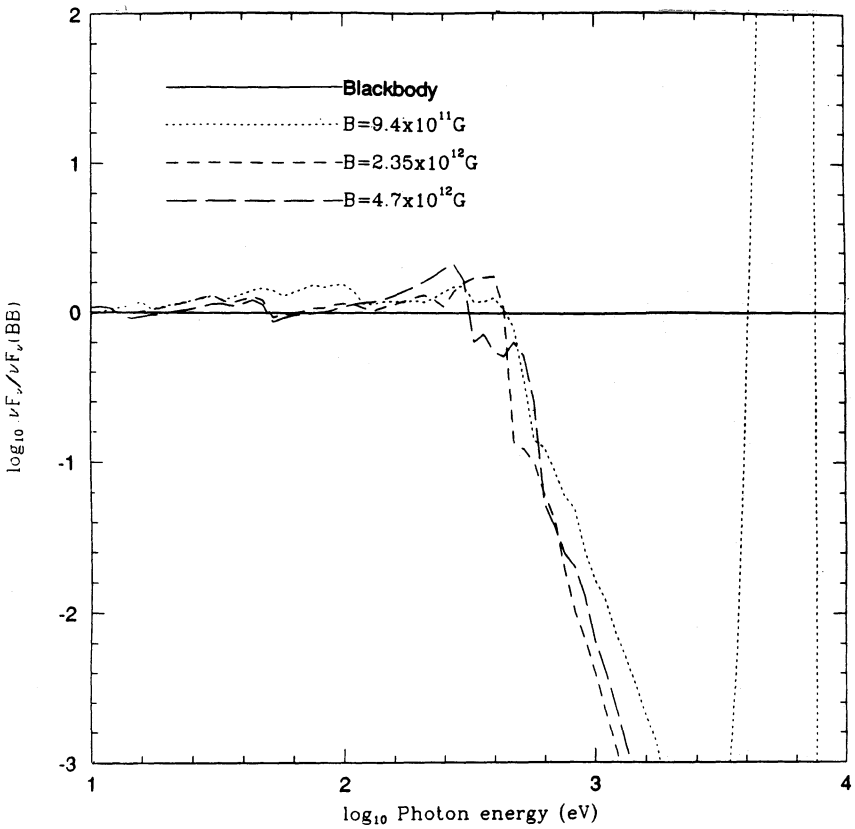

Figure 6. The ratio of the unredshifted spectrum of carbon to the spectrum of a blackbody at $T_{\rm eff} = 1.0 \times 10^6$ K and $B = 9.4 \times 10^{11}$, 2.35×10^{12} and 4.7×10^{12} G.

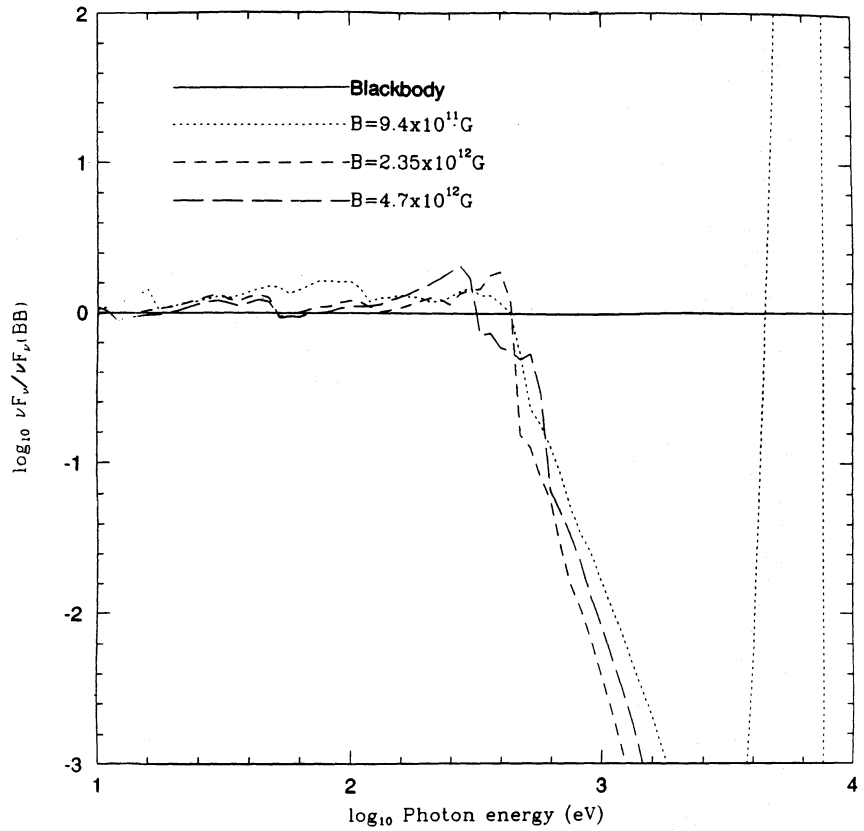

Figure 7. The ratio of the unredshifted spectrum of nitrogen to the spectrum of a blackbody at $T_{\rm eff} = 1.0 \times 10^6$ K and $B = 9.4 \times 10^{11}$, 2.35×10^{12} and 4.7×10^{12} G.

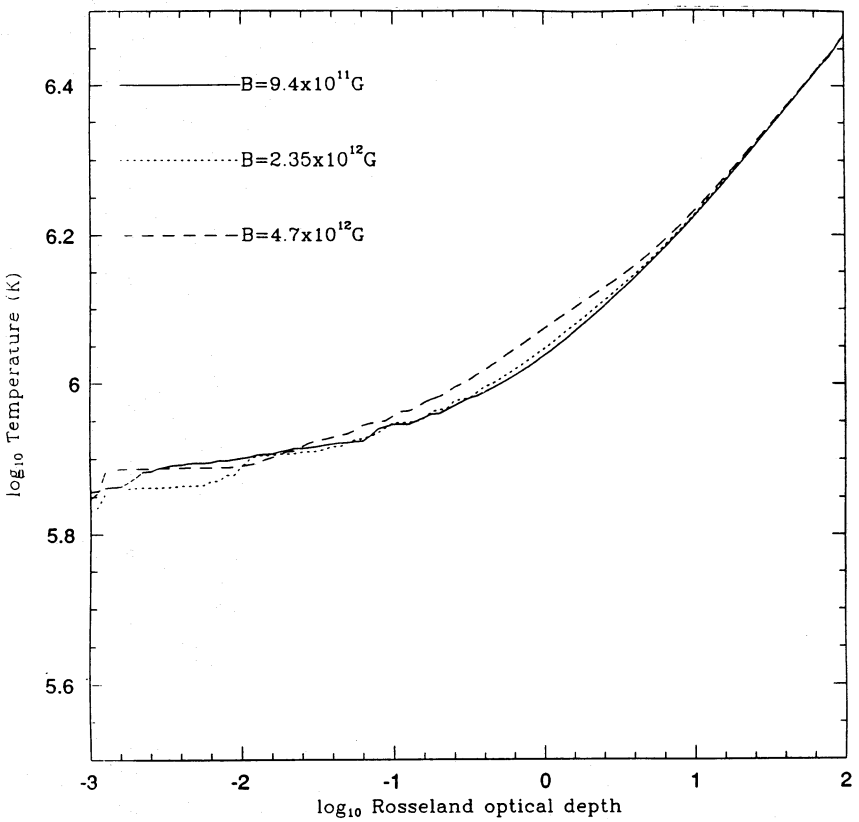

Figure 8. Temperature versus Rosseland optical depth for carbon at an effective temperature of $T_{\rm eff} = 10^6$ K at equatorial magnetic field strengths of $B = 9.4 \times 10^{11}$, 2.35×10^{12} and 4.7×10^{12} G. The relation of temperature to optical depth for other elements is almost identical to that of carbon.

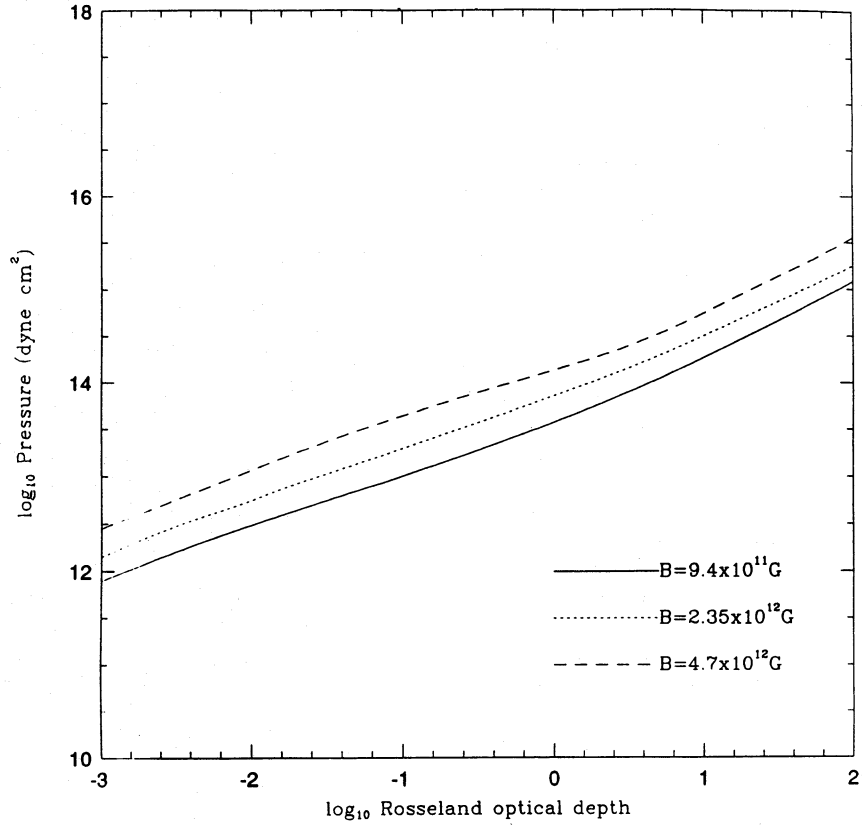

Figure 9. Pressure versus Rosseland optical depth for carbon at an effective temperature of $T_{\rm eff} = 10^6$ K, at equatorial magnetic field strengths of $B = 9.4 \times 10^{11}$, 2.35×10^{12} and 4.7×10^{12} G. The relation of pressure to optical depth for other elements is almost identical to that of carbon.

Table 1. A list of the blackbody temperatures associated with the various magnetic field values and surface compositions of the model atmospheres. In this table, T_E is defined as the temperature of the blackbody curve which gives the same number of counts in the sensitivity range of the *Einstein* IPC (0.5 to 5.0 keV) as the spectrum does, while T_R is defined similarly for the *ROSAT* HRI (0.1 to 2.0 keV).

B(Gauss)	$T_{\rm eff}$(K)	Surface Composition	T_E	T_R
9.4×10^{11}	10^6	H	1.3×10^6	9.3×10^5
		He	8.7×10^6	1.1×10^6
		C	7.8×10^5	1.1×10^6
		N	7.8×10^5	1.1×10^6
2.35×10^{12}	10^6	H	1.3×10^6	1.0×10^6
		He	8.7×10^5	1.1×10^6
		C	7.1×10^5	1.1×10^6
		N	7.1×10^5	1.1×10^6
4.7×10^{12}	10^6	H	1.0×10^6	1.1×10^6
		He	8.3×10^5	1.1×10^6
		C	7.4×10^5	1.1×10^6
		N	7.6×10^5	1.1×10^6

temperature is very close to 1, with a minimum of 0.71 and a maximum of 1.3. This is in contrast to the results of Romani (1987), who found that for $B=0$ the temperature of a blackbody with the same number of counts in the *Einstein* band as the model atmosphere could be much higher than the effective temperature of the star. This is due to two effects which increase the opacity. First, the presence of a magnetic field shifts the energy levels of atoms upward so that the ionization edge is closer to the observed frequencies, which means that the opacity is higher. Second, in a strong field the bound–free cross-section drops off as ν^{-2}, not ν^{-3} as in the non-magnetic case. Since the opacity is higher, the levels of the atmosphere which contribute to the spectrum are higher up, and consequently are cooler. Therefore, the flux is much closer to the blackbody flux at the frequencies of interest.

Except in a few cases, X-ray observations of pulsars have provided only upper limits to their thermal flux. Exceptions include RCW 103, with an estimated blackbody temperature of 2.7×10^6 K (Tuohy & Garmire 1980); PSR 1929+10, with $T_{\rm BB} \approx 2.0 \times 10^5$ K (Helfand 1983); and PSR 0656+14, with $T_{\rm BB} \approx 3-6 \times 10^5$ K (Cordova *et al.* 1989). Non-magnetic calculations indicated that the presence of an atmosphere could significantly affect the resultant surface temperature of these objects. In particular, if the surface temperature is much less than the blackbody temperature the star will have had to cool more quickly than is expected in the standard cooling model [see Tsuruta (1986) for a review]. This may mean that the interior of neutron stars is composed of exotic states of matter such as pion condensates or quark matter, or it may just mean that effects in the standard model such as reheating of the star by differential superfluid rotation (see, e.g. Shibazaki & Lamb 1989) or the importance of the direct URCA process (Lattimer *et al.* 1991) have not been fully taken into account.

Our results seem to indicate that the presence of an atmosphere does not significantly modify the apparent blackbody temperature. This, combined with the new results in the standard cooling picture (e.g. Shibazaki & Lamb 1989; Lattimer *et al.* 1991), indicates that there is, as yet, no evidence for the presence of exotic matter in neutron stars.

ACKNOWLEDGMENTS

Sterl Phinney provided many valuable insights into the physics of this problem. The comments of an anonymous referee were helpful in clarifying the paper. This work was partially supported by NSF grant AST 84-51725 and the Physics Department of the University of Illinois, and was done in partial fulfilment of the PhD requirements at the California Institute of Technology.

REFERENCES

Abrahams, A. M. & Shapiro, S. L., 1991. *Astrophys. J.*, **374,** 652.
Abramowitz, M. & Stegun, I. A., 1972. *Handbook of Mathematical Functions,* Dover, New York.
Alcock, C. & Illarionov, A., 1980. *Astrophys. J.*, **235,** 534.
Battacharya, D. & van den Heuvel, E. P. J., 1991. *Phys. Repts,* **203,** 1.
Collins, G. W., 1988. *Mon. Not. R. astr. Soc.*, **234,** 417.
Cordova, F., Hjellming, R. M., Mason, K. O. & Middleditch, J., 1989. *Astrophys. J.*, **345,** 451.
Forster, H., Strupat, W., Rösner, W., Wunner, G., Ruder, H. & Herold, H., 1984. *J. Phys. B: At. Mol. Phys.*, **17,** 1301.
Harnden, F. R., Fabricant, D. G., Harris, D. E. & Schwarz, J., 1984. *Smithsonian Astrophys. Obs. Spec. Rep.*, No. 393.
Helfand, D. J., 1983. In: *Supernova Remnants and Their X-ray Emission,* p. 471, eds Danziger, J. & Gorenstein, P., Reidel, Dordrecht.
Joss, P. C. & Rappaport, S. A., 1984. *Ann. Rev. Astr. Astrophys.*, **22,** 537.
Kara, S. M. & McDowell, M. R. C., 1980. *J. Phys. B: At. Mol. Phys.*, **13,** 1337.
Khersonskij, V. K., 1987. *Astr. Zh.*, **64,** 433.
Kirk, J. G. & Trümper, J., 1983. In: *Accretion Driven Stellar X-ray*

Sources, p. 261, eds Lewin, W. H. G. & van den Heuvel, E. P. J., Cambridge University Press, Cambridge.
Landau, L. D. & Lifshitz, E. M., 1977. *Quantum Mechanics (Non-relativistic Theory)*, 3rd edn, Pergamon, Oxford.
Lattimer, J. M., Pathick, C. J., Prakash, M. & Haensel, P., 1991. *Phys. Rev. Lett.*, **66**, 2701.
Mihalas, D., 1978. *Stellar Atmospheres*, Freeman, San Francisco.
Miller, M. C. & Neuhauser, D., 1991. *Mon. Not. R. astr. Soc.*, **253**, 107 (Paper I).
Murakami, T. *et al.*, 1988. *Nature*, **335**, 234.
Nagase, F., 1989. *Publs astr. Soc. Japan*, **41**, 1.
O'Connel, R. F., 1979. *Phys. Lett. A*, **70**, 389.
Romani, R. W., 1987. *Astrophys. J.*, **313**, 718.
Rosat mission description, 1989. *NRA 89-OSSA-2 Appendix F*, Rosat Scientific Data Centre, Munich.
Rösner, W., Herold, H., Ruder, H. & Wunner, G., 1983. *Phys. Rev. A*, **28**, 2071.
Rösner, W., Wunner, G., Herold, H. & Ruder, H., 1984. *J. Phys. B: At. Mol. Phys.*, **17**, 29.
Ruder, H., Herold, H., Rösner, W. & Wunner, G., 1985. *Physica B&C*, **127**, 11.
Rybicki, G. B. & Lightman, A. P., 1979. *Radiative Processes in Astrophysics*, Wiley, New York.
Shibazaki, N. & Lamb, F., 1989. *Astrophys. J.*, **346**, 808.
Simola, J. & Virtamo, J., 1978. *J. Phys. B: At. Mol. Phys.*, **11**, 3309.
Tsuruta, S., 1986. *Comm. Astrophys.*, **11**, 151.
Tuohy, I. & Garmire, G., 1980. *Astrophys. J. Lett.*, **239**, L107.
Wunner, G., 1986. *J. Phys. B: At. Mol. Phys.*, **19**, 1623.
Wunner, G. & Ruder, H., 1987. *Phys. Scripta*, **36**, 291.
Wunner, G., Ruder, H. & Herold, H., 1980. *J. Phys. B: At. Mol. Phys.*, **14**, 765.

APPENDIX A: CALCULATION OF THE POLARIZATION COEFFICIENTS

Assuming that the source of radiation is initially isotropic and unpolarized, what fraction of the light that reaches the observer is right-circular, left-circular and B polarized after interacting with the atom? Our coordinates are set up so that the z-axis is along the line-of-sight, and the magnetic field is in the y–z plane and makes an angle of ψ with the z-axis. We assume that the initial ray comes from a direction that makes an angle of θ with the line-of-sight and ϕ with the x-axis. Since the initial ray is unpolarized, it has equal components along both directions perpendicular to the initial direction. To determine the polarization coefficients γ_B, γ_+ and γ_-, we integrate the projections of these components along the $\hat{\boldsymbol{e}}_B$, $_+$ and $_-$ directions, multiplied by a weight function and normalized.

If we assume that the magnetic field is given by

$$\boldsymbol{B} = B_0 \hat{\boldsymbol{e}}_B, \tag{53}$$

where

$$\hat{\boldsymbol{e}}_B = (0, \sin\psi, \cos\psi), \tag{54}$$

then the polarization unit vectors are given by

$$\hat{\boldsymbol{e}}_B = (0, \sin\psi, \cos\psi), \tag{55}$$

$$\hat{\boldsymbol{e}}_+ = \frac{1}{\sqrt{2}}(1, i\cos\psi, -i\sin\psi), \tag{56}$$

$$\hat{\boldsymbol{e}}_- = \frac{1}{\sqrt{2}}(1, -i\cos\psi, i\sin\psi). \tag{57}$$

The initial direction of the ray is

$$\hat{\boldsymbol{e}} = (\cos\phi\sin\theta, \sin\phi\sin\theta, \cos\theta), \tag{58}$$

so the initial polarization will be composed of

$$\boldsymbol{\varepsilon}_{\perp 1} = \frac{1}{\sqrt{2}}(\sin\phi, -\cos\phi, 0) \tag{59}$$

and

$$\boldsymbol{\varepsilon}_{\perp 2} = \frac{1}{\sqrt{2}}(\cos\theta\cos\phi, \cos\theta\sin\phi, -\sin\theta), \tag{60}$$

so that

$$|\boldsymbol{\varepsilon}_{\perp 1}|^2 + |\boldsymbol{\varepsilon}_{\perp 2}|^2 = 1.$$

Following Collins (1988) we note that the electric field of the incoming wave will cause the atom to oscillate, and this motion coupled with the magnetic field will cause a secondary oscillation. Thus, the atom may be considered to have a dipole moment consisting of two parts,

$$\boldsymbol{D} = \boldsymbol{D}_{\rm E} + \boldsymbol{D}_{\rm M}, \tag{61}$$

where

$$\boldsymbol{D}_{\rm E} \propto \boldsymbol{E} \tag{62}$$

and

$$\boldsymbol{D}_{\rm M} \propto \boldsymbol{E} \times \boldsymbol{x}, \tag{63}$$

where

$$\boldsymbol{x} = \left(\frac{e\boldsymbol{B}}{m_{\rm N} c}\right) \Big/ \omega = \frac{\omega_{\rm c}}{\omega}\hat{\boldsymbol{e}}_B, \tag{64}$$

and $m_{\rm N}$ is the mass of the nucleus. Since the gyrofrequency of the nucleus, $\omega_{\rm c}$, is only ≈ 6 eV at $B = 10^{12}$ G (and we will typically consider frequencies higher than that), we will expand only to first order in $x = |\boldsymbol{x}|$.

The new (unnormalized) components of polarization are

$$\hat{\boldsymbol{e}}_{\perp 1} = \frac{1}{\sqrt{2}}[\boldsymbol{\varepsilon}_{\perp 1} + x(\boldsymbol{\varepsilon}_{\perp 1} \times \hat{\boldsymbol{e}}_B)] \tag{65}$$

and

$$\hat{\boldsymbol{e}}_{\perp 2} = \frac{1}{\sqrt{2}}[\boldsymbol{\varepsilon}_{\perp 2} + x(\boldsymbol{\varepsilon}_{\perp 2} \times \hat{\boldsymbol{e}}_B)]. \tag{66}$$

The normalization for both of these is roughly $1/\sqrt{1+x^2}$, which we will approximate as 1.

To get the polarization coefficients, we note that, e.g.,

$$\gamma_B = \int_0^{2\pi}\int_0^{\pi} (|\hat{\boldsymbol{e}}_B \cdot \hat{\boldsymbol{e}}_{\perp 1}|^2 + |\hat{\boldsymbol{e}}_B \cdot \hat{\boldsymbol{e}}_{\perp 2}|^2) \times \omega(\theta, \phi, \psi)\sin\theta\, d\theta\, d\phi / N, \tag{67}$$

where N is the normalization factor and $w(\theta, \phi, \psi)$ is a weight factor [such as $w(\theta, \phi, \psi) = 1 + \cos^2\theta$ for Thomson scattering]. To check the validity of these assumptions, we will first calculate the polarization coefficients for the

isotropic case, $w(\theta, \phi, \psi) = 1$:

$$\gamma_B = \frac{1}{2}\int_0^{2\pi}\int_0^{\pi}(\cos^2\phi\sin^2\psi + \cos^2\theta\sin^2\phi\sin^2\psi \quad (68)$$

$$+ \sin^2\theta\cos^2\psi - 2\sin\theta\cos\theta\sin\phi\sin\psi\cos\psi)$$

$$\times \sin\theta\, d\theta\, d\phi/4\pi = \frac{1}{3} + \mathcal{O}(x^2),$$

$$\gamma_+ = \frac{1}{4}\int_0^{2\pi}\int_0^{\pi}[\sin^2\phi + \cos^2\phi\cos^2\psi + \cos^2\theta\cos^2\phi \quad (69)$$

$$+ \cos^2\theta\sin^2\phi\cos^2\psi + \sin^2\theta\sin^2\psi$$

$$+ 2\sin\theta\cos\theta\sin\phi\sin\psi\cos\psi + \mathcal{O}(x)]\sin\theta\, d\theta\, d\phi/4\pi$$

$$= \frac{1}{3} + \mathcal{O}(x^2),$$

$$\gamma_+ = \gamma_-, \quad (70)$$

so the coefficients are all equal, as they should be. Note that the terms of order x integrate to 0.

As indicated in the previous section, for bound–free absorption the cross-section that is due to B polarization is much greater than that due to circular polarization. This is the case we will consider, but we note in passing that for bound–bound absorption this assumption is decidedly incorrect, since transition rules may forbid absorption that is due to B polarization at certain frequencies. Thus, in a treatment of radiative transfer that includes energies less than the binding energy of the atom, the full formula for polarization coefficients given below with $r > 0$ must be used.

The differential cross-section for unpolarized light may be determined by adding the differential cross-sections that are due to the two polarization components (see e.g. Rybicki & Lightman 1979, p. 90 and following):

$$\frac{d\sigma}{d\Omega} \propto (1 - \hat{e}_{\perp 1,z}^2)\{(\hat{\boldsymbol{e}}_{\perp 1}\cdot\hat{\boldsymbol{e}}_B)^2 + r[1 - (\hat{\boldsymbol{e}}_{\perp 1}\cdot\hat{\boldsymbol{e}}_B)^2]\} \quad (71)$$

$$+ (1 - \hat{e}_{\perp 2,z}^2)\{(\hat{\boldsymbol{e}}_{\perp 2}\cdot\hat{\boldsymbol{e}}_B)^2 + r[1 - (\hat{\boldsymbol{e}}_{\perp 2}\cdot\hat{\boldsymbol{e}}_B)^2]\},$$

where $r \equiv \sigma_+/\sigma_B$ and $\hat{e}_{\perp 1,z}$ is the z-component of the first polarization vector. For an isotropic cross-section, $r = 1$, while for our case, $r \ll 1$. The weight function is

$$w(\theta, \phi, \psi) \propto \frac{d\sigma}{d\Omega}, \quad (72)$$

and the normalization factor is

$$N = \int_0^{2\pi}\int_0^{\pi} w(\theta, \phi, \psi)\sin\theta\, d\theta\, d\phi = \quad (73)$$

$$\frac{\pi}{15}[36(1 - \mathrm{r})\sin^2\psi + 8(1 - r)\cos^2\psi + 80r].$$

The coefficients become

$$\gamma_B = \frac{1}{2}\int_0^{2\pi}\int_0^{\pi}[\cos^2\phi\sin^2\psi + \cos^2\theta\sin^2\phi\sin^2\psi$$

$$+ \sin^2\theta\cos^2\psi - 2\sin\theta\cos\theta\sin\phi\sin\psi$$

$$\times cos\,\psi]\, w(\theta, \phi, \psi)\sin\theta\, d\theta\, d\phi/N$$

$$= \frac{\frac{4}{7}(1 - r) + \frac{22}{7}(1 - r)\sin^2\psi + r(6 + \sin^2\psi)}{2(1 - r) + 7(1 - r)\sin^2\psi + 20r} + \mathcal{O}(x^2), \quad (74)$$

$$\gamma_+ = \gamma_- = \frac{1}{2}(1 - \gamma_B). \quad (75)$$

Notice that, miraculously, x only shows up in terms of order x^2 or higher.

For example, for $\psi = 0$ and $r = 0$, this gives

$$\gamma_B = \frac{2}{7}, \qquad \gamma_+ = \gamma_- = \frac{5}{14}, \quad (76)$$

and for $\psi = \pi/2$ and $r = 0$,

$$\gamma_B = \frac{26}{63}, \qquad \gamma_+ = \gamma_- = \frac{37}{126}. \quad (77)$$

The average value for γ_B over the surface of a neutron star with a dipolar field and a rotation axis aligned with the magnetic axis is about 0.40. The total bound–free cross-section has the form

$$\sigma_{\mathrm{bf}} \sim \gamma_+\sigma_+ + \gamma_-\sigma_- + \gamma_z\sigma_z, \quad (78)$$

so the cross-sections are on average about 20 per cent greater than in the isotropic case.

APPENDIX B: PROJECTED AREA OF THE SURFACE ELEMENTS OF THE STAR

In order to calculate the thermal spectrum of a neutron star properly, we need to figure out how much of the projected surface area of the star has a magnetic field strength in a range dB around B, calculate the spectrum from that area, and integrate over the star. In this appendix, we use Newtonian straight-line optics. For a real neutron star, general relativity would have to be used, which would increase the apparent area of the star. We work with coordinates set up so that the z-axis is lined up with the magnetic axis and the line-of-sight is defined to be in the x–z plane. The projected area of a surface element at a direction (θ, ϕ) is its real area times the dot product of its normal vector with the vector of the line-of-sight. Let

$$\hat{\boldsymbol{r}} = (\sin\theta\cos\phi, \sin\theta\sin\phi, \cos\theta) \quad (79)$$

be the normal vector of the surface element, and

$$\hat{\boldsymbol{q}} = (\sin\psi, 0, \cos\psi) \quad (80)$$

be the vector of the line-of-sight, where ψ is the angle between the magnetic axis and the line-of-sight. Then the contribution from the surface element is

$$\hat{\boldsymbol{r}}\cdot\hat{\boldsymbol{q}} = \sin\theta\cos\phi\sin\psi + \cos\theta\cos\psi. \quad (81)$$

To determine the projected area of the surface with a given magnetic field, we first need to determine how much is visible, since the star will block out its own back side. For a given ψ and θ the range of observable ϕs is determined by the solutions to $\hat{\boldsymbol{r}}\cdot\hat{\boldsymbol{q}}=0$:

$$\cos\phi = -\frac{\cos\theta\cos\psi}{\sin\theta\sin\psi}, \tag{82}$$

so ϕ runs from $-\phi_1$ to ϕ_1, where

$$\phi_1 = \cos^{-1}\left[-\frac{\cos\theta\cos\psi}{\sin\theta\sin\psi}\right]. \tag{83}$$

When the expression in brackets is less than -1, the allowed angles run from $-\pi$ to π, whereas when the expression is greater than $+1$, there are no allowed angles. For a dipolar field, the magnetic field strength is given by

$$|B| = B_{\rm eq}\sqrt{1+3\cos^2\theta}, \tag{84}$$

where $B_{\rm eq}$ is the equatorial field. Thus, if the field varies in strength from B_1 to B_2, the angle varies from

$$\theta_1 = \cos^{-1}\sqrt{\frac{1}{3}\left(\frac{B_1}{B_{\rm eq}}\right)^2 - 1}, \tag{85}$$

to

$$\theta_2 = \cos^{-1}\sqrt{\frac{1}{3}\left(\frac{B_2}{B_{\rm eq}}\right)^2 - 1}. \tag{86}$$

The band from $\pi-\theta_1$ to $\pi-\theta_2$ also encompasses these fields, so the total projected area is

$$A(B_1,B_2) = \int_{\theta_1}^{\theta_2}\int_{-\phi_1}^{\phi_1}(\sin\theta\cos\phi\sin\psi+\cos\theta\cos\psi) \times\sin\theta\,d\phi\,d\theta + \int_{\pi-\theta_2}^{\pi-\theta_1}\int_{\phi_1-\pi}^{\pi-\phi_1}(\sin\theta\cos\phi\sin\psi +\cos\theta\cos\psi)\sin\theta\,d\phi\,d\theta. \tag{87}$$

If θ_1 and θ_2 are close together, we may approximate this double integral by setting $\theta=(\theta_1+\theta_2)/2$, so that

$$A(B_1,B_2)\approx(\theta_2-\theta_1)\sin\theta\left[\int_{-\phi_1}^{\phi_1}(\sin\theta\cos\phi\sin\psi +\cos\theta\cos\psi)\,d\phi + \int_{\phi_1-\pi}^{\pi-\phi_1}(\sin\theta\cos\phi\sin\psi -\cos\theta\cos\psi)\,d\phi\right], \tag{88}$$

where the minus sign in the second integral is because $\cos(\pi-\theta)=-\cos\theta$. In our simulations we use 10 intermediate fields to approximate the surface, though there was almost no difference between using 10 and five.